ACS APPLIED MATERIALS & INTERFACES

Research Article

www.acsami.org

Valence State Control and Third-Order Nonlinear Optical Properties of Copper Embedded in Sodium Borosilicate Glass

Weidong Xiang,* Haihong Gao, Li Ma, Xin Ma, Yunyun Huang, Lang Pei, and Xiaojuan Liang

College of Chemistry and Materials Engineering, Wenzhou University, Wenzhou 325035, China

Supporting Information

ABSTRACT: The integrated and transparent sodium borosilicate glasses that contain copper exhibiting different colors, that is, red, green, and blue were synthesized by combining the sol−gel process and heat treatment in H_2 gas. To reveal substantially the cause of different colors in the glass, X-ray diffraction (XRD), transmission electron microscopy (TEM) and high resolution TEM (HRTEM) were systematically applied to investigate and determine the microstructure of the doped matter. The results showed three different crystals had formed in the red, green and blue glass, and the sizes of these crystals were range from 9 to 34, 1 to 6, and 1 to 5 nm, respectively. The valence state of copper was further analyzed by X-ray photoelectron spectroscopy (XPS) and electron energy loss spectroscopy (EELS). The third-order nonlinear optical properties of the glasses were investigated by using Z-scan technique at the wavelength of 800 nm. Interestingly, the third-order nonlinear absorption of the red, green, and blue glass can be successfully controlled from reverse saturable absorption, no absorption to saturable absorption and the optical nonlinear susceptibility $\chi^{(3)}$ of the red, green and blue glass were estimated to be 6.4×10^{-14}, 1.6×10^{-14}, and 2.6×10^{-14} esu in the single-pulse energy of 0.36 μJ, respectively.

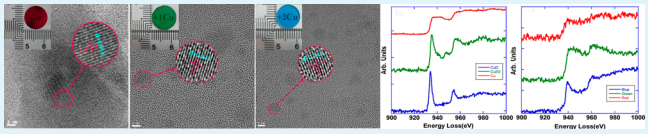

KEYWORDS: *sol−gel, sodium borosilicate glass, microstructure, Z-scan technique*

1. INTRODUCTION

As is well-known, borosilicate glass has higher chemical durability compared to ordinary glass. The remarkably low thermal expansion coefficient (~3.3×10^{-6} °C^{-1} at room temperature) endows borosilicate glass eminent resistance to thermal shock and breaking.[1,2] Such superior properties make borosilicate glass widely used in laboratory equipment and optical devices. Sodium borosilicate glass prepared by sol−gel and heat treatment method undergoes the phase change of solution—xerogel—glass, during which chemicals can be easily doped and well dispersed, porous structure can be naturally formed and substances doped can be well encapsulated and preserved. Therefore, borosilicate glass is a competent base glass to load quantum dots or nanoparticles.

Metal nanoparticles can be embedded in the solid transparent dielectric layer to avoid reuniting and forming the thermodynamics of bulk materials. The electronic density of states, quantum effect, and dielectric confinement[3] endow them unique optical, electrical, magnetic, chemical, and thermal properties.[4] Therefore, the facile preparation and effective characterization of the new nano structural materials (metal-dielectric nanocomposite) with excellent optical performance can greatly promote the modern nano technology and nano photonics research.[5−8] Glass, because of its advantageous characteristics such as good transparency, high mechanical strength, easy processing and preventing the air oxidation of metal nanoparticles, is widely used as an ideal encapsulation materials of metal nanoparticles. Nano metallic glass composites have attracted researchers' great attention, not only because they can be applied to photochromic materials,[9] colored glass circulation industry[10] and three-dimensional color crafts,[11] but also because of their great potential applications in nonlinear optical materials,[12,13] such as optical data recording disks and storage devices,[10,11] optical waveguide,[10,11] and all-optical switches.[7,10−12] In all these applications, the particle size, shape, number density, and distribution of nanoparticles together determine the characteristics and performance of the nanometer composite materials. Numerous studies have shown that metal nanoparticles can significantly enhance the third-order nonlinear optical properties of glass, the third-order nonlinear optical susceptibility was reported to be the largest 10^{-6} esu so far,[14] the response time to be picosecond level,[15,16] and the excellent nonlinear properties attribute to the surface plasmon resonance of the metal nanoparticles[17] and quantum size effect.[18]

As an important transition metal element, copper has a face-centered cubic lattice and a cube crystal cell, with the lattice constant of $a = b = c$ and $\alpha = \beta = \gamma = 90°$. Over the past 5 years, there has been a growing focus on research of copper embedded in glass matrices.[19,21] Cu has an unparalleled price advantage and application prospect, its superior third-order nonlinear optical properties[19,20] and the unique decorative effect of Cu nanoparticles exhibiting red in the glass[22] make it exist great potential application value in the field of nonlinear optics. However, Cu nanoparticles can be introduced into the glass substrate using different methods, such as sol−gel,[23−25]

Received: January 8, 2015
Accepted: April 30, 2015
Published: April 30, 2015

DOI: 10.1021/acsami.5b00218
ACS Appl. Mater. Interfaces 2015, 7, 10162−10168

high temperature melting method,[26,27] ion implantation,[28,29] ion exchange method,[30,31] femtosecond laser irradiation method,[32,33] electric field assisted method,[34,35] etc. Study on Cu quantum dots in the field of nonlinear optics also has attracted great attention due to its distinct physical and chemical properties. The third order nonlinear susceptibility $\chi^{(3)}$ of the Cu nanoclusters in silica glass was determined to be 3.2×10^{-7} esu at 532 nm and 1.7×10^{-7} esu at 1064 nm, respectively.[30]

The valence shell structure of Cu is $3d_{10}4s_1$, therefore the valence of Cu can exhibit 0, +1, and +2, nevertheless, controlling the chemical valence state of Cu freely in the glass is still very difficult, especially the +1 of Cu. Different valence states of copper can show different colors in the glass, so the research of this aspect is very interesting. In this Research Article, we carried out a detailed study on the valence state control of Cu in sodium borosilicate glass synthesized by combining the sol–gel process and heat treatment in different atmosphere.

2. EXPERIMENTAL SECTION

2.1. Preparation of the Glass. The $Na_2O–B_2O_3–SiO_2$ glasses containing copper exhibiting three different colors were fabricated by employing sol–gel and atmosphere control methods. The composition of sodium borosilicate glass matrix was $5Na_2O–20B_2O_3–75SiO_2$ (in wt %). The preparation process was as follows: First, SiO_2 component was obtained by room temperature hydrolysis of tetraethyl orthosilicate (TEOS) in anhydrous ethanol containing deionized water and nitric acid (HNO_3) (pH = 2, as catalyst). Second, B_2O_3 and Na_2O were derived from dissolving boric acid (H_3BO_3) and metallic sodium (Na) in 2-methoxyethanol and anhydrous ethanol, respectively. Then, the two obtained precursor solutions were added into the well hydrolyzed TEOS solution. All chemicals were added according to the designed proportion of the glass composition. After the mixed solution was stirred for 1 h at room temperature, an ethanol solution of copper nitrate ($Cu(NO_3)_3{\cdot}3H_2O$, 2 wt %) was added to form the homogeneously mixed substrate glass solution containing copper. Subsequently, the mixed solution was dried at 80 °C for 3 weeks to form the stiff gel. Finally the stiff gel was heat-treated in tube furnace under different atmospheres according to the following steps: First, the stiff gel was heated in oxygen (O_2) atmosphere at the heating rate of 5 °C·h^{-1} up to 400 °C, and kept for 10 h at 400 °C to remove organic matter and decompose copper nitrate. Second, the xerogel was exposed to dry hydrogen (H_2, 99.99%) at 400 °C for 10 h, 5 and 0 h to form metallic Cu, Cu_2O, and CuO, respectively. Finally, the loose and porous xerogel was heated in nitrogen (N_2) atmosphere at a rate of 10 °C·h^{-1} from 400 to 600 °C, and kept for 5 h at 600 °C. At last, the red, green, and blue well-densified $Na_2O–B_2O_3–SiO_2$ glasses containing Cu, Cu_2O, and CuO were obtained. The glass samples cut and polished are shown in Figure 1a–c.

2.2. Characterization. To explore whether the crystalline structure had formed in the glass, X-ray diffraction analysis of the well cut and polished glasses was performed on a Germany Bruker X-ray diffractometer (40 kV, 20 mA) using Cu Ka radiation (λ = 0.15418 nm) at a scan rate of 0.02° s^{-1} in the range of 15–80°. The glass samples for TEM were prepared by crushing the glass pieces in agate mortar and pestle with ethanol, a drop of the suspension was placed onto a copper grid covered with lacy carbon film. Transmission electron microscopy (TEM) imaging was carried out on a FEI Tecnai F-20 transmission electron microscope at an acceleration voltage of 200 kV. JEM-ARM200F tem (JEOL, 200 kV) equipped with Gatan Enfina electron energy loss spectrometer was used to analyze the valence of Cu in different glass samples. High angle annular dark field (HAADF) images were obtained using 40 um condenser lens aperture camera 8 cm length, lead to 31 mrad convergence Angle and half set 80 mrad Angle (180 mrad collection Angle). The collection angle for EELS acquisition was 49 mrad in the equipment. All of the energy spectrum calibration according to the energy threshold C K edges 284 eV. Then, all the spectra were normalized to copper L_3 edge for curve fitting. X-ray photoelectron spectroscopy (XPS) measurement was carried out using AXI ULTRA DLD spectrometer with monochrome Al Ka as the excitation source. The linear optical absorption of the three glasses in the wavelength range of 400–1100 nm was obtained at room temperature by a PerkinElmer Lambda 750 UV–vis Spectrometer. The open-aperture and closed-aperture of the 800 nm Z-scan tests of the red, green and blue glasses were carried out at the repetition rate of 20 Hz, pulse width of 190 fs and single-pulse energy of 0.36, 0.72, and 1.5 μJ.

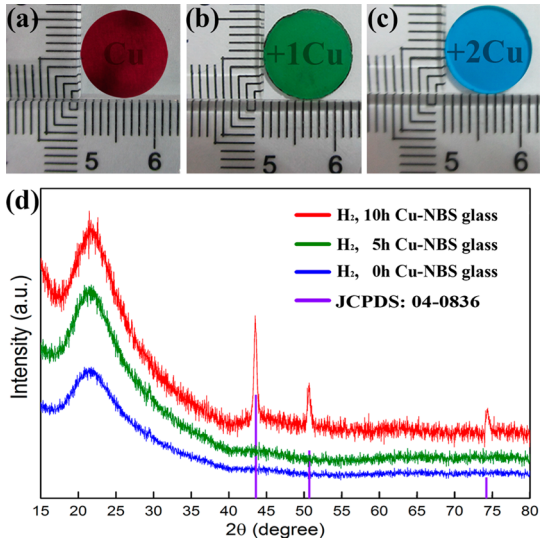

Figure 1. Photograph of as-obtained glass: (a) red glass, (b) green glass, and (c) blue glass. (d) The XRD pattern of the glass.

3. RESULTS AND DISCUSSION

3.1. XRD Analysis. Figure 1a–c shows real photos of as-synthesized transparent red, green, and blue sodium borosilicate glass containing copper, the diameter of which is about 1 cm. To substantially understand the reason why glasses containing copper exhibit different colors, the XRD analysis was performed. Figure 1d shows the XRD pattern of glass samples: the red curve, green curve and blue curve represented the XRD pattern of the red, green and blue sodium borosilicate glass containing copper, respectively. As can be seen from the curves, there was a big baglike amorphous peak while 2θ was about 22° which was caused by the base glass diffraction. The red glass had three sharp peaks. The diffraction planes (111), (200), (220) were in good accordance with the standard card JCPDS No.04-0836, and there was no other impurity peaks, which indicated that pure Cu crystals had formed in the red glass. Sharp diffraction peaks indicated that the crystallization of Cu nanoparticles was very good. The average size of Cu nanoparticles was estimated by Scherrer formula,[36] the calculation formula is

$$d = \frac{K\lambda}{\beta \cos\theta} \quad (1)$$

d represented the average particle size of nanoparticles, λ represented X-ray wavelength, β stood for half peak width (fwhm), θ stood for Bragg diffraction angle, and K was approximately 0.9. We could calculate that the average particle size of Cu nanocrystals in sodium borosilicate glass was about 18.5 nm. The red glass formed Cu crystals under the control of temperature and atmosphere was preliminarily confirmed by

DOI: 10.1021/acsami.5b00218
ACS Appl. Mater. Interfaces 2015, 7, 10162–10168

XRD analysis. The green curve and the blue curve had no signals of diffraction peak except the big baglike amorphous peak, the reason for which could be that no crystals had formed in the green glass and the blue glass or that the crystals formed were too small to lead to agglomeration, causing diffraction peaks broadening and being not obvious. To essentially and precisely find out the truth, the following TEM was applied to have insight into the inner structure of the glass.

3.2. TEM Analysis. To capture the information on the microstructure of the glass samples, TEM analysis was subsequently carried out. Figure 2a–c showed the TEM images

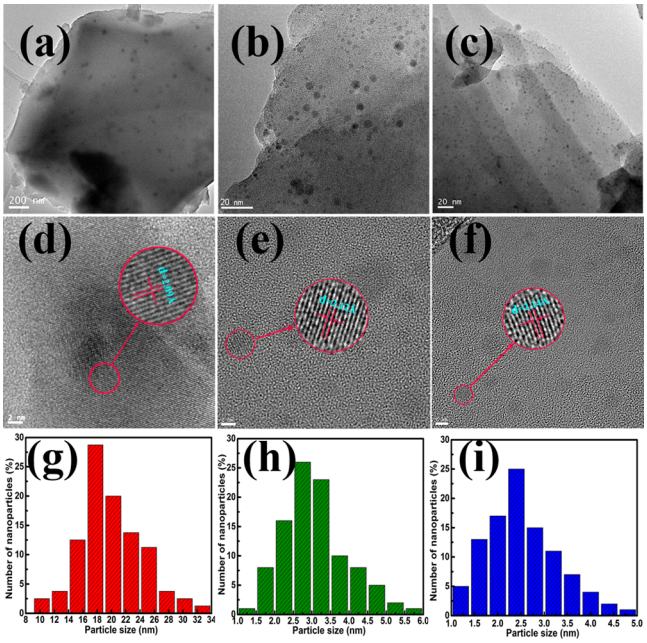

Figure 2. TEM images of the glass samples: (a) red, (b) green, and (c) blue. HRTEM images of the glass samples: (d) red, (e) green, and (f) blue. Size distribution images of (g) red, (h) green, and (i) blue glass, respectively.

of the red, green and blue glass. We were most inspired to find that there were lots of black particles with different size dispersedly embedded in each of the glass substrate in Figure 2a–c. HRTEM was conducted to further conform what exactly the nanoparticles (NPs) in the three glasses were. Figure 2d–f showed the HRTEM images of NPs in red, green, and blue glass, the lattice parameters were respectively measured to be 2.09 Å, 2.12, and 2.14 Å. Compared the measured lattice parameters with those listed in the Cu containing oxides, we found that the lattice of NPs in red glass was close to pure Cu metal (PDF no. 04-0836, 2.088 Å for [111] plane), NPs in green glass seemed to be Cu_2O (PDF no. 34-1354, 2.120 Å for [200] plane), while NPs in the blue glass was comparable to CuO (PDF no. 44-0706, 2.140 Å for [200] plane). The particle size distribution of the NPs in red, green and blue glass is shown in Figure 2g–i, it could be seen that the diameter of the NPs in the red glass was about 9–34 nm, and the average particle diameter of Cu nanoparticles was 18.8 nm. In the green glass the NPs was smaller, the average particle diameter of which was about 3.12 nm; while in blue glass, the size distribution of particles was the most dispersed and average diameter was about 2.24 nm. These results were well in agreement with the XRD analysis. Combined TEM and HRTEM analysis, a preliminary summary could be reached that NPs in the green and the blue glass containing copper in oxidation state were in the range of several nanometers in diameter, which could be the reason why XRD techniques could not be used to quantify the oxidation states of Cu in the sodium borosilicate glass.

3.3. XPS Analysis. XPS was conducted to further confirm the valence state of copper in the three glasses. Figure 3a

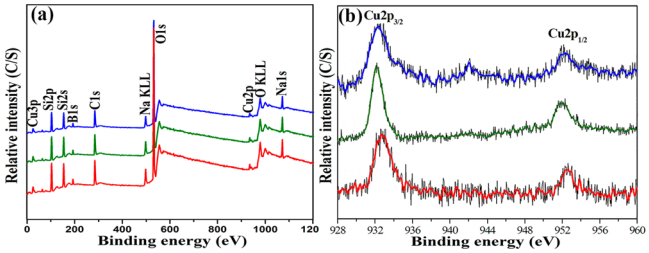

Figure 3. XPS spectra of the red, green and blue NBS glass containing Cu: (a) XPS full spectrum and (b) Cu 2p high-resolution spectrum of the blue, green, and red glass.

showed the survey scan XPS spectra of the glass, in which red, green and blue curves were corresponding to the color of the glass. As seen from the diagram, the glass sample component elements: Na, B, Si, O, and Cu signals were all showed. Figure 3b represented the high resolution X-ray photoelectron spectrum for Cu 2p of the blue, green and red sodium borosilicate glass, in which the spectral line shape of the red glass curve and the green glass curve in Figure 3b was similar including two peaks that corresponded to Cu 2p3/2 and Cu 2p1/2, their binding energy were respectively 932.67 eV, 952.56 and 932.16 eV, 952.12 eV, which indicated the valence state of Cu in the sample was 0 or +1, well consistent with the values reported in the literature.[37,38] However, we could not confirm the valence state was 0 or +1 because the binding energy position of Cu 2p and the spectral line shape of Cu^0 and Cu^{1+} were almost the same.[39] The top curve of the blue glass in Figure 3b had a small peak at 942.11 eV between the two strong peaks, which was the characteristic peak of Cu^{2+},[40] consistent with the HRTEM analysis of the blue glass. To more clearly reveal the valence state of Cu in the glass, especially in the red and green glass, electron energy loss spectrometer (EELS) was used.

3.4. EELS Analysis. Figure 4a was the high angle annular dark field (HAADF) image of the red glass, in which the signal intensity was proportional to the atomic numbers ($I \approx Z^2$, where Z was atomic number and I was the signal intensity),[41] therefore the bright Cu NPs could be clearly visualized in Figure 4a. Figure 4b represented 3D view of the result of EELS linescan from A to B (all spectra were with equal distance and background subtracted for clear view). A distinct peak appeared (as indicated in Figure 4b) which corresponded to Cu edge when the electron probe was moved on to the bright spot in Figure 4a, and disappeared simultaneously when the electron probe moved to glass matrix. All of the three glasses had the same phenomena after repeated examination, which proved that the NPs in NBS glass were Cu rich particles.

The spectrum of Cu-NPs showed in red line at the top of Figure 5a, for its filled 3d orbit, it presented as flat and broad edges of L_3 and L_2 instead of sharp peaks. The medial one in green line represented Cu_2O, besides $L_{2,3}$, there was an extra small peak located in 947.5 eV. The transitions into the Cu 4s states above the Fermi level might be responsible for this

DOI: 10.1021/acsami.5b00218
ACS Appl. Mater. Interfaces 2015, 7, 10162–10168

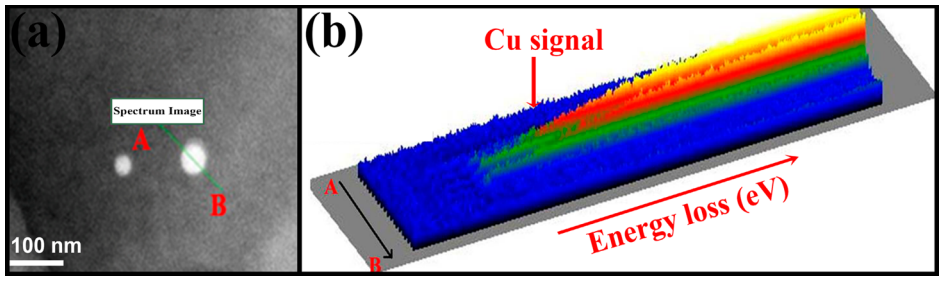

Figure 4. (a) HAADF STEM image of the red glass. The line from A to B shows EELS linescan direction. (b) 3D view of the EELS linescan result.

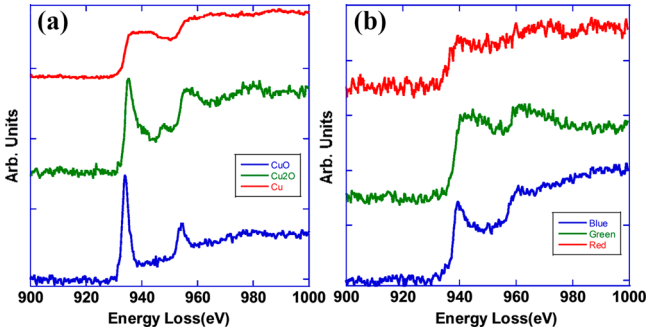

Figure 5. (a) Reference EELS spectra of Cu. (b) The experimental EELS spectra reproduced from Figure 4b.

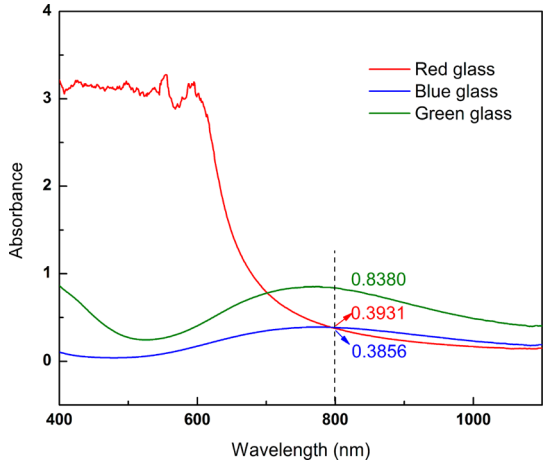

Figure 6. Linear optical absorption spectra of the red, green, and blue glass.

phenomenon.[42,43] The bottom blue line belonged to the EELS spectrum of Cu^{2+}, in which the FWHMs of L_3 and L_2 were smaller than that of Cu^{+}. Figure 5b showed the EELS spectra of $L_{2,3}$ of Cu in the glass. Take the EELS spectra of copper in Figure 5a as reference, the shape of the curves in Figure 5b were very similar to the reference ones. The red line proved metallic Cu existed in the red glass, the green one was consistent with the standard reference of Cu_2O, the result of blue line showed that mainly Cu^{2+} existed in the blue glass. It should be illustrated that the reference EELS spectra of Cu ions with valence of +1 and +2 exhibited a sharp peak, while the experiment EELS spectra shown a broad peak, which may be attribute to the doping concentration of Cu ions in the sodium borosilicate glass was only 2.0 wt % and the response signal was lower than the reference Cu ions. Furthermore, the valence of Cu ions in green and blue glass was not only +1 and +2, respectively, which may be some Cu^{+} in blue glass and Cu^{2+} in green glass. And the further reasons are under way. In a word, combined with XRD, HRTEM, and XPS analysis, the main NPs in the red, green and blue glass were finally confirmed to be Cu, Cu_2O and CuO nanocrystal, respectively, and they were mainly embedded in the glass matrix.

3.5. Nonlinear Optical Property. To determine the nonlinear refraction and absorption of the copper doped sodium borosilicate glass samples, linear absorbance (in Figure 6), open aperture (OA) and closed aperture (CA) Z-scan measurements were carried out. Figure 7 represented open-aperture ($S = 1$) and closed-aperture ($S = 0.05$) Z-scan results with single-pulse energy of 0.36 μJ for $Na_2O-B_2O_3-SiO_2$ glass containing Cu, Cu_2O and CuO NPs, respectively. Here the black squares in the figure indicated the experimental result while solid line for theoretical fit of the normalized transmittance. Figure 7a–c showed that the OA of Cu, Cu_2O, and CuO NPs doped glass. Figure 7a was symmetric relative to the focus ($z = 0$) where it had minimum transmittance of the red glass, illustrating reverse saturable absorption would occur in the red glass, Figure 7b showed no sign of nonlinear absorption while OA of CuO doped glass in Figure 7c suggested a saturable absorption would occur in the blue glass. Figure 7d–f displayed the CA of the copper doped glasses. The CA Z-scan curves with prefocal ($Z < 0$) minimum and the postfocal ($Z > 0$) maximum indicated a self-focusing process and a positive sign of nonlinear refractive index ($\gamma > 0$). Both nonlinear absorption coefficient (β) and nonlinear refractive index (γ) of the glasses were calculated from the OA and CA Z-scan curves according to the well-known theory.[44] The real and imaginary parts of the third-order nonlinear susceptibility were deduced according to the parameters β and γ, as shown in eqs 2 and 3.[45]

$$\mathrm{Im}\,\chi^{(3)}\ (\mathrm{esu}) = \frac{\lambda\varepsilon_0 c^2 {n_0}^2}{4\pi^2}\beta(m/W) \tag{2}$$

$$\mathrm{Re}\chi^{(3)}\ (\mathrm{esu}) = \frac{\varepsilon_0 c^2 {n_0}^2}{\pi}\gamma(m^2/W) \tag{3}$$

λ, ε_0, c, and n_0 are the wavelength of the laser light, permittivity of free space, speed of light, and linear refractive index of the glass, respectively. The total optical third-order nonlinear susceptibility $\chi^{(3)}$ is given by eq 4.[46]

$$|\chi^{(3)}|\ (\mathrm{esu}) = \{(\mathrm{Re}\chi^{(3)})^2 + (\mathrm{Im}\chi^{(3)})^2\}^{1/2} \tag{4}$$

All of the nonlinear parameters are listed in Table 1. Obviously, the introduction of Cu, Cu_2O, and CuO nanocrystals in sodium borosilicate glass would result in different third-order nonlinear properties of the glass. For example, when Cu^0 presented in the glass, the third-order nonlinear absorption was reverse saturable and the third-order nonlinear susceptibility was as high as 6.4×10^{-14} esu, which was the maximum of the

DOI: 10.1021/acsami.5b00218
ACS Appl. Mater. Interfaces 2015, 7, 10162–10168

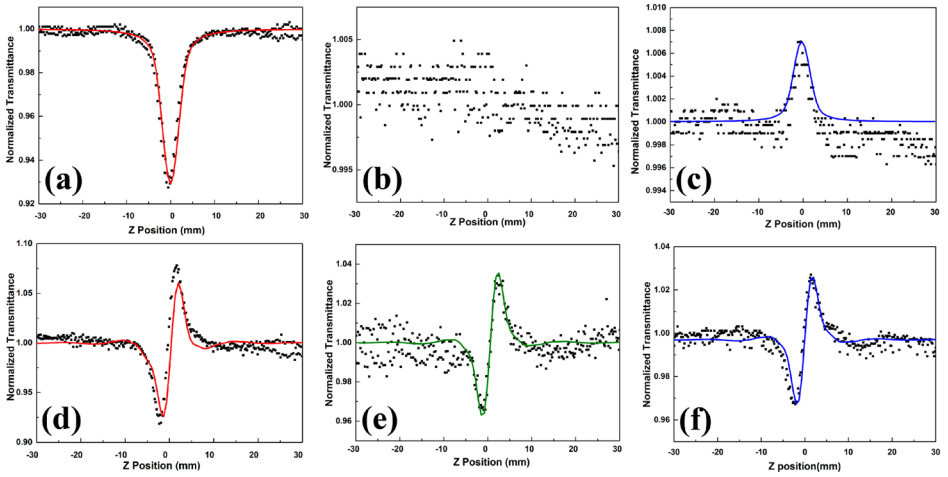

Figure 7. Z-scan normalized transmittance curves of the glasses with single-pulse energy of 0.36 μJ: (a) open-aperture Z-scan curve of the red glass; (b) open-aperture Z-scan curve of the green glass; (c) open-aperture Z-scan curve of the blue glass; (d) closed-aperture Z-scan curve of the red glass; (e) closed-aperture Z-scan curve of the green glass; (f) closed-aperture Z-scan curve of the blue glass. (Theoretical data in black squares and fitting curves in solid line).

Table 1. Third-Order Nonlinear Optical Parameters of the Three Glasses at 800 nm with Single-Pulse Energy of 0.36 μJ

parameters	γ (m^2/w)	Re$\chi^{(3)}$(esu)	β(m/w)	Im$\chi^{(3)}$(esu)	$\chi^{(3)}$(esu)
Cu^0	5.3×10^{-20}	2.9×10^{-14}	4.1×10^{-13}	5.7×10^{-14}	6.4×10^{-14}
Cu^{1+}	2.9×10^{-20}	1.6×10^{-14}	0	0	1.6×10^{-14}
Cu^{2+}	4.2×10^{-20}	2.3×10^{-14}	-8.0×10^{-14}	1.1×10^{-14}	2.6×10^{-14}

three glass samples. While Cu^{2+} doped in the glass, it turned out to be saturable absorption and the third-order nonlinear susceptibility reached 1.6×10^{-14} esu. The Z-scan test with single-pulse energy of 0.72 and 1.5 μJ showed similar results and they are presented in Supporting Information Figures S2 and S3.

4. CONCLUSION

In summary, the integrated and transparent red, green and blue copper containing sodium borosilicate glasses were successfully synthesized by the sol−gel and oxidation and reduction atmosphere control methods. On the basis of XRD and TEM analysis, Cu, Cu_2O, and CuO nanocrystals were found in the red, green, and blue glass matrix and the average sizes of these crystals were 18.8 nm, 3.12 and 2.24 nm, respectively. XPS and EELS analysis further revealed the valence state of copper were mainly 0, +1, and +2 in red, green, and blue glass, respectively. Therefore, the red, green, and blue colors of the glass respectively correspond to Cu (Cu^0), Cu_2O (Cu^{1+}), and CuO (Cu^{2+}) nanocrystals doped in the glass. The convenient quantitative doping of copper and effective control of heat treatment atmosphere contribute greatly to the successful synthesis of Cu, Cu_2O, and CuO nanocrystals doped colored glass and pave a way in valence control of metallic element in preparation and modification of new materials. In addition, the nonlinear optical properties of the glasses were determined using Z-scan and the results indicated that the glass had excellent third-order optical nonlinearities, the $\chi^{(3)}$ of the red, green and blue glass were measured to be 6.4×10^{-14}, 1.6×10^{-14}, and 2.6×10^{-14} esu, respectively. In addition, the adjustment of nonlinear absorption of the copper doped sodium borosilicate glass from reverse saturable absorption to saturable absorption in the single-pulse energy range of 0.36−1.5 μJ by controlling the valence state of copper was realized. Therefore, the glasses may have potential applications in the field of nonlinear optics with further improvement.

■ ASSOCIATED CONTENT

Ⓢ Supporting Information

Supplementary experimental results and supporting data, including SAED patterns and Z-scan results with singe-pulse energy of 0.72 and 1.5 μJ of the red, green, and blue glass samples. The Supporting Information is available free of charge on the ACS Publications website at DOI: 10.1021/acsami.5b00218.

■ AUTHOR INFORMATION

Corresponding Author

*Tel: +86-577-86596013. Fax: +86-577-86689644. E-mail: xiangweidong001@126.com.

Notes

The authors declare no competing financial interest.

■ ACKNOWLEDGMENTS

The work was financially supported by the Zhejiang Province Natural Science Foundation (LQ14E020006) and National Nature Science Foundation of China (51272059, 51472183 and 51172165).

■ REFERENCES

(1) Axinte, E. Glasses as Engineering Materials: A Review. *Mater. Des.* **2011**, *32*, 1717−1732.

(2) Forde, L. C.; Proud, W. G.; Walley, S. M.; Church, P. D.; Cullis, I. G. Ballistic Impact Studies of a Borosilicate Glass. *Int. J. Impact Eng.* **2010**, *37*, 568−578.

(3) Speranza, G.; Minati, L.; Chiasera, A.; Ferrari, M. G.; Righini, C.; Ischia, G. Quantum Confinement and Matrix Effects in Silver-Exchanged Soda Lime Glasses. *J. Phys. Chem. C* **2009**, *113*, 4445−4450.

DOI: 10.1021/acsami.5b00218
ACS Appl. Mater. Interfaces 2015, 7, 10162−10168

(4) Prasad, P. N. In *Nanophotonics*; Prasad, P. N., Ed.; Wiley: Hoboken, NJ, 2004; Chapter 4, pp 79−127.
(5) Zhang, Y.; Chen, Y.; Shi, L.; Li, J.; Guo, Z. Recent Progress of Double-structural and Functional Materials with Special Wettability. *J. Mater. Chem.* **2012**, *22*, 799−815.
(6) Yang, L.; Wang, S.; Mao, J.; Deng, J.; Gao, Q.; Tang, Y.; Schmidt, O. G. Hierarchical MoS_2/Polyaniline Nanowires with Excellent Electrochemical Performance for Lithium-Ion Batteries. *Adv. Mater.* **2013**, *25*, 1180−1184.
(7) Silva-Pereyra, H.; Arenas-Alatorre, J.; Rodriguez-Fernández, L.; Crespo-Sosa, A.; Cheang-Wong, J.; Reyes-Esqueda, J.; Oliver, A. High Stability of the Crystalline Configuration of Au Nanoparticles Embedded in Silica under Ion and Electron Irradiation. A. *J. Nanopart. Res.* **2010**, *12*, 1787−1795.
(8) Shi, C.; Soltani, S.; Armani, A. M. Gold Nanorod Plasmonic Upconversion Microlaser. *Nano Lett.* **2013**, *13*, 5827−5831.
(9) Korgel, B. A. Materials Science: Composite for Smarter Windows. *Nature* **2013**, *500*, 278−279.
(10) Chen, S.; Akai, T.; Kadono, K.; Yazawa, T. Reversible Control of Silver Nanoparticle Generation and Dissolution in Soda-Lime Silicate Glass through X-Ray Irradiation and Heat Treatment. *Appl. Phys. Lett.* **2001**, *79*, 3687−3689.
(11) Zeng, H.; Qiu, J.; Ye, Z.; Zhu, C.; Gan, F. Irradiation Assisted Fabrication of Gold Nanoparticles-Doped Glass. *J. Cryst. Growth* **2004**, *267*, 156−160.
(12) Mangin, S.; Gottwald, M.; Lambert, C. H.; Steil, D.; Uhlíř, V.; Pang, L.; Hehn, M.; Alebrand, S.; Cinchetti, M.; Malinowski, G.; Fainman, Y.; Aeschlimann, M.; Fullerton, E. E. Engineered Materials for All-Optical Helicity-Dependent Magnetic Switching. *Nat. Mater.* **2014**, *13*, 286−292.
(13) Llordés, A.; Garcia, G.; Gazquez, J.; Milliron, D. J. Tunable Near-Infrared and Visible-Light Transmittance in Nanocrystal-in-Glass Composites. *Nature* **2013**, *500*, 323−326.
(14) Ryasnyansky, A. I.; Palpant, B.; Debrus, S.; Khaibullin, R. I.; Stepanov, A. L. Nonlinear Optical Properties of Copper Nanoparticles Synthesized in Indium Tin Oxide Matrix by Ion Implantation. *J. Opt. Soc. Am. B* **2006**, *23*, 1348−1353.
(15) Heidt, A. M.; Li, Z.; Sahu, J.; Shardlow, P. C.; Becker, M.; Rothhardt, M.; Ibsen, M.; Phelan, R.; Kelly, B.; Alam, S. U.; Richardson, D. J. 100 kW Peak Power Picosecond Thulium-Doped Fiber Amplifier System Seeded by a Gain-Switched Diode Laser at 2 μm. *Opt. lett.* **2013**, *38*, 1615−1617.
(16) Li, R. K.; To, H.; Andonian, G.; Feng, J.; Polyakov, A.; Scoby, C. M.; Thompson, K.; Wan, W.; Padmore, H. A.; Musumeci, P. Surface-Plasmon Resonance-Enhanced Multiphoton Emission of High-Brightness Electron Beams from a Nanostructured Copper Cathode. *Phys. Rev. Lett.* **2013**, *110*, No. 074801.
(17) Hou, W.; Cronin, S. B. A Review of Surface Plasmon Resonance-Enhanced Photocatalysis. *Adv. Funct. Mater.* **2013**, *23*, 1612−1619.
(18) Jiang, F.; Chen, D.; Li, R.; Wang, Y.; Zhang, G.; Li, S.; Zheng, J.; Huang, N.; Gu, Y.; Wang, C.; Shu, C. Eco-Friendly Synthesis of Size-Controllable Amine-Functionalized Graphene Quantum Dots with Antimycoplasma Properties. *Nanoscale* **2013**, *5*, 1137−1142.
(19) Krishna, M. B. M.; Kumar, V. P.; Venkatramaiah, N.; Venkatesan, R.; Rao, D. N. Nonlinear Optical Properties of Covalently Linked Graphene−Metal Porphyrin Composite Materials. *Appl. Phys. Lett.* **2011**, *98*, No. 081106.
(20) Ray, P. C. Size and Shape Dependent Second Order Nonlinear Optical Properties of Nanomaterials and Their Application in Biological and Chemical Sensing. *Chem. Rev.* **2010**, *110*, 5332−5365.
(21) Wang, Y. H.; Liu, F.; Cheng, H.; Yu, X. X.; Wei, L. Third Order Non-Linear Optical Response of Cu Nanoclusters by Ion Implantation in Silicate Glass under 532 and 1064 nm Laser Excitations. *Mater. Res. Innovations* **2014**, *18*, 241−244.
(22) Colomban, P. The Use of Metal Nanoparticles to Produce Yellow, Red and Iridescent Colour, from Bronze Age to Present Times in Lustre Pottery and Glass: Solid State Chemistry, Spectroscopy and Nanostructure. *J. Nano Res.* **2009**, *8*, 109−132.
(23) Reisfeld, R.; Grinberg, M.; Levchenko, V.; Kukliński, B.; Mahlik, S.; Magdassi, S.; Grouchko, M. Sol−Gel Glasses with Enhanced Luminescence of Laser Dye Rhodamine B Due to Plasmonic Coupling by Copper Nanoparticles. *Opt. Mater.* **2014**, *36*, 1611−1615.
(24) Ruivo, A.; Ventura, M. G.; Gomes da Silva, M. D. R; Laia, C. Synthesis of Gold Nanoparticles in Sol−Gel Glass Porogens Containing [bmim][BF_4] Ionic Liquid. *J. Sol−Gel Sci. Technol.* **2013**, *68*, 234−244.
(25) Russo, L.; Gabrielli, L.; Valliant, E. M.; Nicotra, F.; Jiménez-Barbero, J.; Cipolla, L.; Jones, J. R. Novel Silica/Bis(3-Aminopropyl) Polyethylene Glycol Inorganic/Organic Hybrids by Sol−Gel Chemistry. *Mater. Chem. Phys.* **2013**, *140*, 168−175.
(26) Dousti, M. R.; Sahar, M.; Amjad, R. J.; Ghoshal, S.; Awang, A. Surface Enhanced Raman Scattering and Up-Conversion Emission by Silver Nanoparticles in Erbium−Zinc−Tellurite Glass. *J. Lumin.* **2013**, *143*, 368.
(27) Chen, F.; Dai, S.; Xu, T.; Shen, X.; Lin, C.; Nie, Q.; Liu, C.; Heo, J. Surface-Plasmon Enhanced Ultrafast Third-Order Optical Nonlinearities in Ellipsoidal Gold Nanoparticles Embedded Bismuthate Glasses. *Chem. Phys. Lett.* **2011**, *514*, 79−82.
(28) Stepanov, A.; Galyautdinov, M.; Evlyukhin, A.; Nuzhdin, V.; Valeev, V.; Osin, Y.; Evlyukhin, E.; Kiyan, R.; Kavetskyy, T.; Chichkov, B. Synthesis of Periodic Plasmonic Microstructures with Copper Nanoparticles in Silica Glass by Low-Energy Ion Implantation. *Appl. Phys. A: Mater. Sci. Process.* **2013**, *111*, 261−264.
(29) Srivastava, S.; Gangopadhyay, P.; Amirthapandian, S.; Sairam, T.; Basu, J.; Panigrahi, B.; Nair, K. Effects of High-Energy Si Ion-Irradiations on Optical Responses of Ag Metal Nanoparticles in a SiO_2 Matrix. *Chem. Phys. Lett.* **2014**, *607*, 100−104.
(30) Karvonen, L.; Rönn, J.; Kμjala, S.; Chen, Y.; Säynätjoki, A.; Tervonen, A.; Svirko, Y.; Honkanen, S. High Non-Resonant Third-Order Optical Nonlinearity of Ag-Glass Nanocomposite Fabricated by Two-Step Ion Exchange. *Opt. Mater.* **2013**, *36*, 328−332.
(31) Toda, I.; Tsuruoka, T.; Matsui, J.; Murashima, T.; Nawafune, H.; Akamatsu, K. In Situ Synthesis of Metal/Polymer Nanocomposite Thin Films on Glass Substrates by Using Highly Cross-Linked Polymer Matrices with Tailorable Ion Exchange Capabilities. *RSC Adv.* **2014**, *4*, 4723−4726.
(32) Almeida, J. M. P.; De Boni, L.; Avansi, W.; Ribeiro, C.; Longo, E.; Hernandes, A. C.; Mendonca, C. R. Generation of Copper Nanoparticles Induced by fs-Laser irradiation in borosilicate glass. *Opt. Express* **2012**, *20*, 15106−15113.
(33) Liu, K.; Yang, Q.; Zhao, Y.; Chen, F.; Shan, C.; He, S.; Fan, X.; Meng, X.; Du, G.; Bian, H. Three-Dimensional Metallic Microcomponents Achieved in Fused Silica by a Femtosecond-Laser-Based Microsolidifying Process. *Microelectron. Eng.* **2014**, *113*, 93−97.
(34) Chhowalla, M.; Shin, H. S.; Eda, G.; Li, L. J.; Loh, K. P.; Zhang, H. The Chemistry of Two-Dimensional Layered Transition Metal Dichalcogenide Nanosheets. *Nat. Chem.* **2013**, *5*, 263−275.
(35) Horikoshi, S.; Osawa, A.; Abe, M.; Serpone, N. On the Generation of Hot-Spots by Microwave Electric and Magnetic Fields and Their Impact on a Microwave-Assisted Heterogeneous Reaction in the Presence of Metallic Pd Nanoparticles on an Activated Carbon Support. *J. Phys.Chem. C* **2011**, *115*, 23030−23035.
(36) Patterson, A. The Scherrer Formula for X-Ray Particle Size Determination. *Phys. Rev.* **1939**, *56*, 978−982.
(37) Zhang, Q.; Gao, T.; Andino, J. M.; Li, Y. Copper and Iodine Co-Modified TiO_2 Nanoparticles for Improved Activity of CO_2 Photo Reduction with Water Vapor. *Appl. Catal. B: Environ.* **2012**, *123*, 257−264.
(38) Jacob, K.; Stolle, A.; Ondruschka, B.; Jandt, K. D.; Keller, T. F. Cu on Porous Glass: An Easily Recyclable Catalyst for the Microwave-Assisted Azide-Alkyne Cycloaddition in Water. *Appl. Catal., A* **2013**, *451*, 94−100.
(39) Fiermans, L.; Hoogewijs, R.; Vennik, J. Electron Spectroscopy of Transition Metal Oxide Surfaces. *Surf. Sci.* **1975**, *47*, 1−40.
(40) Akhavan, O.; Ghaderi, E. Copper Oxide Nanoflakes as Highly Sensitive and Fast Response Self-Sterilizing Biosensors. *J. Mater. Chem.* **2011**, *21*, 12935−12940.

DOI: 10.1021/acsami.5b00218
ACS Appl. Mater. Interfaces 2015, 7, 10162−10168

(41) Pennycook, S.; Boatner, L. Chemically Sensitive Structure-Imaging with a Scanning Transmission Electron Microscope. *Nature* **1988**, *336*, 565−567.
(42) Leapman, R.; Grunes, L. Anomalous L_3L_2 White-Line Ratios in the 3d Transition Metals. *Phys. Rev. Lett.* **1980**, *45*, 397−401.
(43) Shao, Y.; Maunders, C.; Rossouw, D.; Kolodiazhnyi, T.; Botton, G. A. Quantification of the Ti Oxidation State in $BaTi_{1-x}Nb_xO_3$ Compounds. *Ultramicroscopy* **2010**, *110*, 1014−1019.
(44) Sheik-Bahae, M.; Said, A. A.; Wei, T.-H.; Hagan, D. J.; Van Stryland, E. W.; Wei, T. H.; et al. Sensitive Measurement of Optical Nonlinearities Using a Single Beam. *IEEE J. Quantum Electron.* **1990**, *26*, 760−769.
(45) Fan, G.; Ren, S.; Qu, S.; Guo, Z.; Wang, Q.; Wang, Y.; Gao, R. Mechanisms for Fabrications and Nonlinear Optical Properties of Pd and Pt Nanoparticles by Femtosecond Laser. *Opt. Commun.* **2013**, *295*, 219−225.
(46) Wang, Y. H.; Wang, Y. M.; Lu, J. D.; Ji, L. L.; Zang, R. G.; Wang, R. W. Nonlinear Optical Properties of Cu Nanoclusters by Ion Implantation in Silicate Glass. *Opt. Commun.* **2010**, *283*, 486−489.

DOI: 10.1021/acsami.5b00218
ACS Appl. Mater. Interfaces 2015, 7, 10162−10168